Asociación Argentina
de Mecánica Computacional

Mecánica Computacional Vol XXXVII, págs. 983-992 (artículo completo)
A. Cardona, L. Garelli, J.M. Gimenez, P.A. Kler, S. Márquez Damián, M.A. Storti (Eds.)
Santa Fe, 5-7 Noviembre 2019

MODELING OF IGNITION PROCESS FOR PREMIXED COMBUSTION IN A CONSTANT VOLUME BOMB

Joaquín Aranciaga[a], Ezequiel J. López[a] and Norberto M. Nigro[b]

[a]*Instituto de Investigación en Tecnologías y Ciencias de la Ingeniería, Universidad Nacional del Comahue-CONICET, Buenos Aires 1400, 8300 Neuquén, Argentina, joaquin.aranciaga@gmail.com, ezequiel.lopez@fain.uncoma.edu.ar*

[b]*Centro de Investigación en Métodos Computacionales, Universidad Nacional del Litoral-CONICET, Predio CONICET "Dr. Alberto Cassano", Colectora RN 168 s/n – Paraje El Pozo, 3000 Santa Fe, Argentina, norberto.nigro@cimec.santafe-conicet.gov.ar*

Keywords: Computational Fluid Dynamics, Premixed Combustion, Ignition, Extended Coherent Flame Model, OpenFOAM®.

Abstract. Computational Fluid Dynamics is a widespread tool employed in the design of Internal Combustion Engines (ICE), mainly focused to improve efficiency and reduce pollutant emissions. Given the complexity associated with solving turbulent, multiphase, chemically reacting flows, many models have been proposed to represent as accurate as possible phenomena taking place inside ICE, keeping computational costs below reasonable levels. Specifically, mixture ignition and initial flame kernel development are decisive factors affecting the whole combustion process in spark-ignition engines, and current ignition models are not able to correctly predict the flame behavior when ICE operative conditions are varied, making it a subject that has drawn attention over the last years. In the present work, an ignition model taken from the literature named ISSIM (Imposed Stretch Spark Ignition Model), originally developed for LES (Large Eddy Simulation) is implemented in OpenFOAM® and adapted here to work with eddy viscosity models using RANS (Reynolds-Average Navier-Stokes) equations. Ignitions of air-propane mixtures in a constant volume bomb are simulated for different equivalence ratios and turbulent intensity levels, analyzing the dependence of the solution on the electrical parameters of the spark-ignition system. Results are contrasted with experimental data selected from the literature, and furthermore, advantages and drawbacks are discussed compared to other ignition models used in common practice.

1 INTRODUCTION

Much efforts have been allotted to improving ICE (Internal Combustion Engine) efficiency and reducing pollutant emissions for the last decades, becoming increasingly important nowadays due to the stringent regulations imposed by regulatory authorities around the world. In this sense, Spark-Ignition (SI) Engines operating with lean mixtures are being investigated to fulfill those requirements, and CFD (Computational Fluid Dynamics) has proven considerable helpful to predict the responses to changes in operating conditions. As vital processes as they are, ignition and flame kernel development must be accurately modeled when attempting to reproduce experimental data such as pressure or heat fluxes temporal records, in order to validate the code and to trust its consequent results. Several models with varying degrees of complexity have been proposed for igniting the mixture, but to the authors' knowledge either they are formulated in such a simplistic way that there is no means they can account for changes in basic variables like ignition energy or power (e.g. Choi and Huh, 1998), they attempt to consider the physics but have been unsuccessful in test configurations other than the ones originally evaluated (e.g. Boudier et al., 1992) or their validation cases are not abundant enough to prove their full capabilities (e.g. Duclos and Colin, 2001; Colin and Truffin, 2011; Lucchini et al., 2013). The ignition model ISSIM (Imposed Stretch Spark Ignition Model) originally developed by Colin and Truffin (2011) for LES (Large Eddy Simulation) codes is here adapted for RANS (Reynolds-Average Navier-Stokes) codes. This model was selected because it works with the ECFM (Extended Coherent Flame Model) from the moment of ignition, and still takes consideration of the physics of the discharge. A sensitivity analysis of the ignition energy and equivalence ratio is performed by solving the explosions of propane-air mixtures executed in a constant volume bomb; the results of the model are compared with those given by Lim et al. (1987) for stagnant mixtures. Moreover, the effects of turbulence are evaluated by contrasting with Leed's published data (Bradley et al., 2003).

2 GOVERNING CONSERVATION EQUATIONS

The set of equations to be solved may be found in López et al. (2016), and is repeated here for the sake of completeness. Equations (1) to (3) represent the conservation of mass, momentum and specific enthalpy, respectively, written for a compressible flow (Poinsot and Veynante, 2012), where $\bar{\phi}$ denotes the Reynolds average of a generic variable ϕ, and $\tilde{\phi} = \overline{\rho\phi}/\bar{\rho}$ its Favre averaging.

$$\frac{\partial \bar{\rho}}{\partial t} + \frac{\partial \bar{\rho}\tilde{u}_i}{\partial x_i} = 0 \tag{1}$$

$$\frac{\partial \bar{\rho}\tilde{u}_j}{\partial t} + \frac{\partial \bar{\rho}\tilde{u}_i\tilde{u}_j}{\partial x_i} + \frac{\partial \bar{p}}{\partial x_j} = \frac{\partial}{\partial x_i}\left[(\bar{\mu}+\bar{\mu}_t)\left(\frac{\partial \tilde{u}_i}{\partial x_j} + \frac{\partial \tilde{u}_j}{\partial x_i} - \frac{2}{3}\delta_{ij}\frac{\partial \tilde{u}_k}{\partial x_k}\right)\right] - \frac{2}{3}\frac{\partial \bar{\rho}\tilde{k}}{\partial x_i} \tag{2}$$

$$\frac{\partial \bar{\rho}\tilde{h}}{\partial t} + \frac{\partial \bar{\rho}\tilde{u}_i\tilde{h}}{\partial x_i} + \frac{\partial}{\partial x_i}\left[\left(\frac{\bar{\lambda}}{\bar{c}_p} + \bar{\rho}\bar{\alpha}_t\right)\frac{\partial \tilde{h}}{\partial x_i}\right] = \frac{\partial \bar{p}}{\partial t} - \bar{\rho}\frac{D\tilde{K}}{Dt} \tag{3}$$

where $\bar{\rho}$ is the density, $\tilde{u}_i$ is the i-th velocity component, $\bar{p}$ is the pressure, $\tilde{K}$ and $\tilde{k}$ are the mean and turbulent kinetic energy, respectively, $\bar{\mu}$ and $\bar{\mu}_t$ are the molecular and turbulent dynamic viscosity, respectively, $\tilde{h}$ is the specific enthalpy, $\bar{\lambda}$ is the thermal conductivity, $\bar{\alpha}_t$ is the turbulent thermal diffusivity and $\bar{c}_p$ is the specific heat capacity at constant pressure, and $\delta_{i,j}$ is the Kronecker delta tensor. The combustion process is assumed here to proceed in the flamelet

regime. The normalized fuel mass fraction $\tilde{b}$, also known as the regress variable, tracks the spacial gas distribution, and is solved for by an additional transport equation:

$$\frac{\partial \bar{\rho}\tilde{b}}{\partial t} + \frac{\partial \bar{\rho}\tilde{u}_i\tilde{b}}{\partial x_i} - \frac{\partial}{\partial x_i}\left(\frac{\mu_t}{\sigma_b}\frac{\partial \tilde{b}}{\partial x_i}\right) = -\bar{\rho}_u s_L \Sigma \tag{4}$$

where $\bar{\rho}_u$ is the density of the unburned gas, σ_b is the turbulent Schmidt number for $\tilde{b}$, s_L is the laminar burning velocity and Σ is the flame surface density. In this work, Σ is calculated by solving a transport equation:

$$\frac{\partial \bar{\rho}\Sigma}{\partial t} + \frac{\partial \bar{\rho}\tilde{u}_i\Sigma}{\partial x_i} = \frac{\partial}{\partial x_i}\left(\frac{\mu_t}{\sigma_\Sigma}\frac{\partial \Sigma}{\partial x_i}\right) - \bar{\rho}\Sigma\frac{\partial u_i}{\partial x_i} + \bar{\rho}\left(\kappa_m\Sigma + \kappa_t\Sigma - D_\Sigma\right) \tag{5}$$

where σ_Σ is the turbulent Schmidt number for Σ, κ_m and κ_t are the mean flow and turbulent induced strain rates over the flame surface and D_Σ is a destruction term. As the properties between burned and unburned gas differ vastly, a transport equation for the unburned gas specific enthalpy $\tilde{h}_u$ is appended in order to compute the required unburned gas properties, such as its temperature and density (Colin et al., 2003):

$$\frac{\partial \bar{\rho}\tilde{h}_u}{\partial t} + \frac{\partial \bar{\rho}\tilde{u}_i\tilde{h}_u}{\partial x_i} + \frac{\partial}{\partial x_i}\left[\left(\frac{\bar{\lambda}_u}{\bar{c}_{p,u}} + \bar{\rho}\bar{\alpha}_t\right)\frac{\partial \tilde{h}_u}{\partial x_i}\right] = \frac{\bar{\rho}}{\bar{\rho}_u}\left(\frac{\partial \bar{p}}{\partial t} - \bar{\rho}\frac{D\tilde{K}}{Dt}\right) \tag{6}$$

where $\bar{\lambda}_u$ and $\bar{c}_{p,u}$ are the thermal conductivity and specific heat capacity at constant pressure for the unburned gas, respectively. The turbulence is computed employing the extensively used standard $k-\epsilon$ model (Launder and Spalding, 1974). The unstretched laminar burning velocity is obtained from a correlation proposed by Amirante et al. (2017), which reads:

$$\begin{aligned} s_{L,0}(\phi, T_u, p_u) = s_0\left(\frac{T_u}{T_0}\right)^{\alpha}\left(\frac{p_u}{p_0}\right)^{\beta} \quad ; \quad s_0(\phi) = ZW\phi^{\eta}e^{-\xi(\phi-\sigma)^2} \\ \alpha(\phi) = a_2\phi^2 - a_1\phi + a_0 \quad ; \quad \beta(\phi) = -b_2\phi^2 + b_1\phi - b_0 \end{aligned} \tag{7}$$

In Eq. (7), Z, W, η, ξ, σ, a_2, a_1, a_0, b_2, b_1 and b_0 are coefficients which depend on fuel, and for propane are listed in Table 1; ϕ is the equivalence ratio and s_0 is the unstretched burning velocity for the reference pressure ($p_0 = 1$ atm) and temperature ($T_0 = 298$ K).

Z	W (cm/s)	η	ξ	σ	a_2	a_1	a_0	b_2	b_1	b_0
1	42.11	-0.25	5.24	1.10	2.7620	5.8808	4.9221	0.9250	2.0000	1.3560

Table 1: Coefficients for propane in Eq. (7).

The effects of stretch on the burning velocity are considered through a linear relationship:

$$s_L = s_{L,0}\left(1 - \frac{\bar{\rho}_b}{\bar{\rho}_u}La_bK\right) \tag{8}$$

where La_b is a Markstein length (Bradley et al., 1998), $\bar{\rho}_b$ is the density for the burned gas and $K = \min(\kappa\delta/s_{L,0}, 0.2)$ is a Karlovitz stretch factor, which is limited by above due to the fact that the linear expression applies only for small stretch values. The flame stretch κ is the sum

of curvature, mean flow and turbulence effects, and the laminar flame thickness $\delta = \bar{\mu}/(\bar{\rho} s_{L,0})$ is calculated according to Bradley et al. (1996).

The set of partial differential equations introduced above, and the ignition model to be described in the next section were implemented in OpenFOAM®, which employs the Finite Volume Method (FVM) with a cell-centered collocated variable arrangement. The solver uses a combination of the SIMPLE (Semi-Implicit Method for Pressure-Linked Equations, Patankar (1980)) and PISO (Pressure-Implicit with Splitting Operators, Issa (1986)) algorithms. Gradient schemes for all the fields are discretized using the Green-Gauss theorem with linear interpolation to face centroids, Laplacian schemes are corrected to account for mesh non-orthogonality and divergence schemes are discretized using the divergence theorem, with a limited linear interpolation scheme. The time scheme is Backward Euler, with time step $\Delta t = 1$ μs, selected according to a Δt independence analysis. The mesh is made up of uniformly distributed hexahedra with $\Delta x = 1.125$ mm, determined from considerations of error magnitude versus computational cost (see Figure 1).

3 ISSIM SPARK IGNITION MODEL

The ISSIM ignition model is compound of three stages (Mouriaux, 2016): estimation of ignition energy transferred to the gas, deposit of initial burned gases and growth of the flame kernel.

3.1 Estimation of ignition energy transferred to the gas

The electrical circuit used to predict the energy deposited in the gas is an inductive-type one, with a set of adjustable parameters comprising both primary and secondary inductances (L_p and L_s, respectively), secondary resistance (R_s) and primary peak current i_p. A schematic of such an electrical circuit may be found, for example, in Ge and Zhao (2018). The deposited ignition energy can be computed as:

$$E_{ign}(t) = \int V_{gc}(t) i_s(t) \exp\left(-\frac{d}{2 l_{spk}}\right) dt \tag{9}$$

where i_s is the secondary current, l_{spk} is the spark length and d is the diameter of the electrodes; the exponential factor allows to incorporate the effect of thermal losses to the electrodes, as explained in Mouriaux (2016). The gas column fall for the glow phase, V_{gc}, is obtained from a correlation developed by Pashley et al. (2000):

$$V_{gc} = 396 l_{spk} i_s^{-0.415} p^{0.182} \tag{10}$$

where l_{spk} and i_s are expressed in mm and mA, respectively, and p is the pressure in bar (abs); i_s is related to the energy stored in the secondary coil, E_s, through $i_s(t) = \sqrt{2E_s(t)/L_s}$. The decayment of E_s for the glow phase is due to Joule heating and power provided to the spark gap:

$$\frac{\mathrm{d}E_s(t)}{\mathrm{d}t} = -R_s i_s^2(t) - V_{spk}(t) i_s(t) \quad \text{and} \quad V_{spk}(t) = V_{af} + V_{cf} + V_{gc} \tag{11}$$

where the spark voltage, V_{spk}, is the sum of the anode, cathode and gas column fall. The former two depend on the electrode materials, and are taken here to be 109.4 V and 18.75 V, respectively (Ge and Zhao, 2018); energy provided by these falls is mainly lost to the electrodes. As initial condition for Eq. (11), the energy stored in the primary coil, given by $E_p = \frac{1}{2} L_p i_p^2$, is assumed to be transferred to the secondary coil with a conversion efficiency: $E_s(t=0) = 0.6 E_p$

(Ge and Zhao, 2018). As extremely fast and complex processes, breakdown (BD) and arc phases are accounted for by introducing an instantaneous amount of energy, estimated by averaging the range reported for the BD energy by Lim et al. (1987), and affected by a factor of 0.6 to account for losses.

3.2 Deposit of initial burned gases

A minimum ignition energy (MIE), E_{min}, is assessed according to Mouriaux (2016), where the theory developed in Adelman (1981) is followed:

$$E_{min} = \frac{\gamma}{\gamma - 1} l_{spk}(t) p(t) \pi \delta_L^2 \tag{12}$$

being γ the heat capacities ratio and δ_L the laminar flame thickness, which in this work is obtained from the Blint's correlation (Poinsot and Veynante, 2012). As can be seen in Eq. (12), no turbulent parameter affects MIE, justified by the author for their poorly correlated effects. However, this contradicts some experimental data (Mouriaux, 2016). In addition, the dependence of MIE on the spark gap (or the length of the spark in this case) is linear, while it is known that the relationship highly depends on the *Quenching Distance* (QD) (Lewis and Vol Elbe, 1987). Supporting this concept, Ko et al. (1991) show MIE to increase when reducing gap size below the QD (contradicting Eq. (12)), therefore no gap sensitivity analysis will be performed here. The moment in which the ignition energy surpasses the minimum given by Eq. (12), an initial mass of gases is deposited:

$$m_{bg}^{ign} = \langle \rho_u l_{spk} \pi (2\delta_L^2) \rangle \tag{13}$$

where brackets denote an average in the spark plug region. In order to deposit this burned mass, a target profile for the $\tilde{b}$ field is proposed:

$$\bar{b}_{ign} = 1 - c_0 \exp\left[- \left(\frac{|\mathbf{x} - \mathbf{x_{spk}}|}{d_g} \right)^2 \right] \tag{14}$$

Here $|\mathbf{x} - \mathbf{x_{spk}}|$ is the distance between cell centers and the ignition location, d_g is the spark gap size and c_0 is a constant that satisfies $\int (\bar{\rho}_b (1 - \bar{b}_{ign})) dV = m_{bg}^{ign}$, where $\bar{\rho}_b$ is the burned gas density; this expression should be integrated over the whole domain (the integrand will automatically tend to zero as $\bar{b}_{ign}$ goes to unity, regardless of the pre-existance of some burned volume due, e.g. to a second spark plug). The $\bar{b}_{ign}$ field is now imposed to the $\tilde{b}$ field as a sink term (for the whole domain), which is subtracted to the right-hand side of the general $\tilde{b}$ equation:

$$\overline{\dot{\omega}}_b = \bar{\rho}_u \max(s_L \Sigma, (\tilde{b} - \bar{b}_{ign}) \Delta t^{-1}); \tag{15}$$

In this way, pre-existing flame kernels are also accounted for in the transport equation for $\tilde{b}$.

3.3 Growth of the flame kernel

Since the main idea behind ISSIM is that reaction is modeled by the Σ equation rather than having to use a 0D model with its implications, a source term must be added to the right-hand side of the Σ equation:

$$\overline{\dot{\omega}}_\Sigma = \max(\bar{\rho}(\Sigma_{ign} - \Sigma) \Delta t^{-1}, 0); \tag{16}$$

where Σ_{ign} is the target profile for Σ:

$$\Sigma_{ign} = \frac{3}{r_b^{ign}} (1 - \bar{b}_{ign}) \quad \text{and} \quad r_b^{ign} = \left(\frac{3 m_{bg}^{ign}}{4 \pi \bar{\rho}_b} \right)^{1/3} \tag{17}$$

Integrating Σ_{ign} over the whole domain the total flame surface is recovered, which coincides with the external surface of the burned mass given by Eq. (13). If a kernel with its associated Σ already exists anywhere in the domain (including the ignition location), Eq. (16) will be zero (provided $\Sigma > \Sigma_{ign}$ in that particular point).

Given that the Σ equation is formulated for a fully established turbulent flame front, it is necessary to perform some modifications on it for the developing stage of the flame. An approach similar to the one taken by Choi and Huh (1998) is adopted here, with a transition variable alike the one proposed by Colin and Truffin (2011) for being particularly smooth. The modified equation for Σ is written as follows:

$$\frac{\partial \bar{\rho}\Sigma}{\partial t} + \frac{\partial \bar{\rho}\tilde{u}_i\Sigma}{\partial x_i} = \frac{\partial}{\partial x_i}\left(\frac{\mu_t}{\sigma_\Sigma}\frac{\partial \Sigma}{\partial x_i}\right) - \bar{\rho}\Sigma\frac{\partial u_i}{\partial x_i} + \alpha_{tr}\bar{\rho}(\kappa_m\Sigma + \kappa_t\Sigma - D_\Sigma) + (1-\alpha_{tr})\frac{2}{r_b}(1+\tau)\Xi s_L\bar{\rho}\Sigma + (1-\alpha_{tr})\frac{\partial \bar{\rho}}{\partial t}\Sigma + \overline{\dot{\omega}}_\Sigma \tag{18}$$

where $\tau = \bar{\rho}_u/\bar{\rho}_b - 1$ is the expansion ratio and Ξ is a turbulent wrinkling factor assumed equal to one with the aim to circumvent its complex modeling requirements for the ignition time. This simplification proves adequate for low turbulence intensities. The transition variable α_{tr} is calculated as:

$$\alpha_{tr} = 0.5\left[1 + \tanh\left((r_b^+ - 0.75)/0.15\right)\right] \quad \text{with} \quad r_b^+ = 10 r_b/l_t \tag{19}$$

l_t being the integral length scale of turbulence, and the burned radius r_b obtained from:

$$r_b = \left(\frac{3}{4\pi}\int (1-\tilde{b})\frac{\bar{\rho}}{\bar{\rho}_b}dV\right)^{1/3} \tag{20}$$

The CFM2b (Duclos et al., 1993) model is used to compute the production and destruction terms:

$$\kappa_m\Sigma = A_{ik}\frac{\partial \tilde{u}_k}{\partial x_i}\Sigma \quad ; \quad \kappa_t\Sigma = \alpha_0\Gamma_{\bar{K}}\frac{\tilde{\varepsilon}}{\tilde{k}}\Sigma \quad \text{and} \quad D_\Sigma = \beta_0\frac{s_L + C\sqrt{\tilde{k}}}{\tilde{b}(1-\tilde{b})}\Sigma^2 \tag{21}$$

α_0, β_0 and C are adjustment constants, $\tilde{\varepsilon}$ is the specific turbulent kinetic energy dissipation rate, $A_{ik} = \delta_{ij} - \langle n_i n_j\rangle_s$ correspond to the orientation factors for κ_m, and $\Gamma_{\bar{K}}$ is the efficiency function from ITNFS (Intermittent Turbulent Net Flame Stretch, Meneveau and Poinsot (1991)).

4 RESULTS

4.1 Stagnant tests

Lim et al. (1987) studied explosions in a constant-volume cylindrical bomb, 83 mm of inner diameter and length under stagnant conditions; and they are used here to assess the ability of the ignition model to predict changes in spark ignition energy deposition. The mixture is composed of propane-air with an equivalence ratio of 0.7, and three input energies are compared: 2, 11.5 and 54.8 mJ with discharge durations of 264, 810 and 3730 μs, respectively. As turbulence is neglected for these cases, transition from laminar to turbulent flow never occurs, and all terms multiplied by α_{tr} in Eq. (18) are zero. The direct consequence is that the particular ECFM selected has no effect at all. Figure 2 compares the evolution of the equivalent kernel radii. It can be noted the much higher initial radii set by the model (full lines) compared with

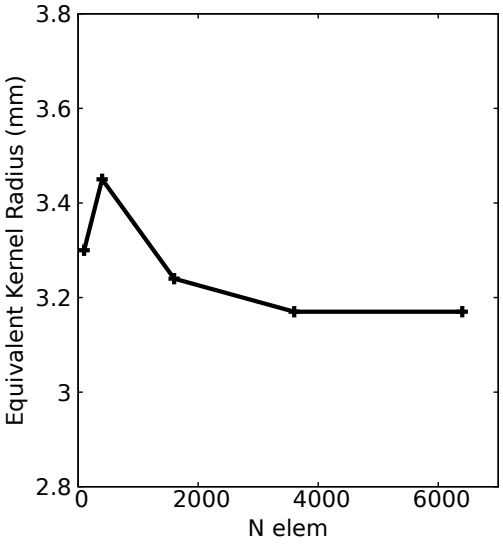

Figure 1: Mesh convergence analysis.

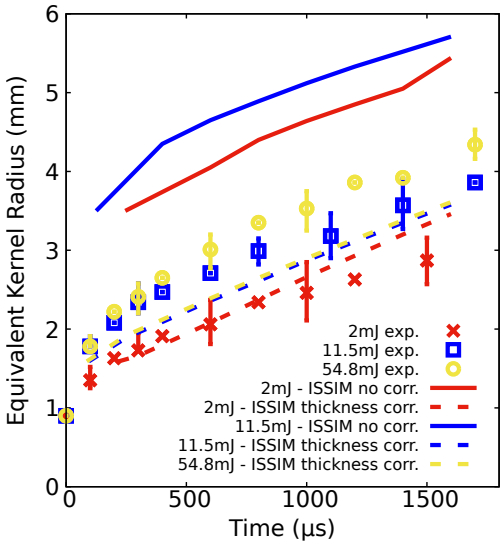

Figure 2: Comparison of predicted and experimental flame kernel radii with and without thickness correction factors. Experimental range for some of the points is represented by vertical bars.

the experimentally observed ones, and this discrepancy remains in time. These are directly attributed to both the laminar flame thickness and the critical radius. The former is computed here using Blint's equation, while in Colin and Truffin (2011) it is not explicitly declared (had they used a diffusive laminar thickness, for example, there would exist a difference by a factor of order 5, approximately). As for the critical radius, it is actually estimated in the original paper (Adelman, 1981), and the author concludes that it lies between one half and four halves of the laminar flame thickness. With this in mind, two factors affecting the laminar flame thickness, $F_{\delta,1}$ and $F_{\delta,2}$, are introduced for the purpose of calculating the minimum energy and initial burned radius:

$$E_{min} = \frac{\gamma}{\gamma - 1} l_{spk}(t) p(t) \pi (F_{\delta,1} \delta_L)^2 \quad \text{and} \quad m_{bg}^{ign} = \langle \rho_u l_{spk} \pi (F_{\delta,2} \delta_L)^2 \rangle \tag{22}$$

The best fits were obtained using $F_{\delta,1} = 0.8$ and $F_{\delta,2} = 0.6$. The flame kernel radii computed using this correction are shown by dashed lines in Figure 2. While these factors may fix the large initial radii, difference in ignition energy is not accurately reflected (curves for the two larger energy levels are almost overlapped), so an ad-hoc coefficient F_i is suggested to modify the laminar flame speed:

$$s_L = s_{L,0}(1 - La_b K)(1 + F_i) \quad \text{with} \quad F_i = 0.15 E_{s,0} \left(\frac{i_s}{i_{s,0}} \right)^2 \exp \left[- \left(\frac{|\mathbf{x} - \mathbf{x_{spk}}|}{d_g} \right)^2 \right] \tag{23}$$

where $E_{s,0}$ is the initial secondary energy in mJ and $i_{s,0}$ the initial secondary current in A. The purpose is to increase the burning velocity through F_i in the vicinity of the spark plug (controlled by the exponential factor), just as long as the spark keeps supplying energy (handled by the non-dimensionalized secondary current). This increment is also thought to depend on the initial available energy ($E_{s,0}$), where a proportional relationship was assumed. Figure 3 demonstrates the effect of this last correction.

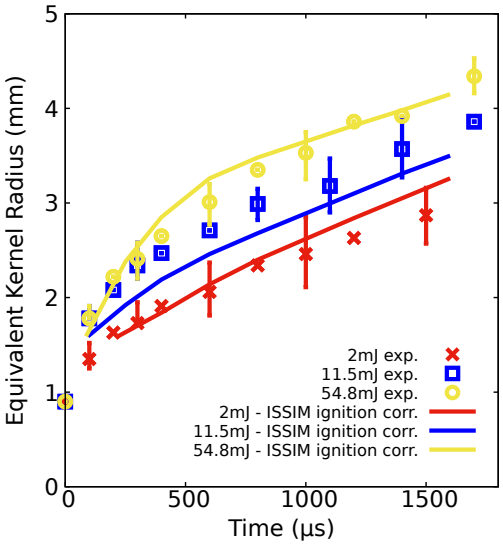

Figure 3: Comparison of predicted and experimental flame kernel radii with the proposed ignition correction factor. Experimental range for some of the points is represented by vertical bars.

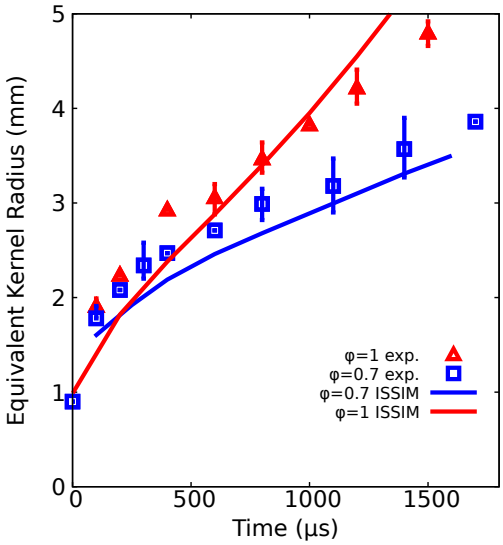

Figure 4: Effect of mixture equivalence ratio on temporal growth of flame kernel radii. Experimental range for some of the points is represented by vertical bars.

As presented in Figure 4, a correct trend is predicted when varying the equivalence ratio; here, an ignition energy of 11.5 mJ was employed for $\phi = 0.7$, and 12.4 mJ for $\phi = 1$.

4.2 Turbulent tests

Results published by Bradley et al. (2003) for explosions inside a constant-volume spherical bomb are compared with predictions of the present model, using the same time step and cell sizes as before. An ignition energy of 23 mJ was reported, while no data was explicitly informed for the duration and gap size, so these had to be estimated for the simulations. Details of the bomb configuration may be found in the cited article. As transition is expected to occur, the ECFM employed will increasingly affect the kernel development as α_{tr} goes from zero to one. The model parameters chosen are: $\alpha_0 = 6$, $\beta_0 = 0.17$, and $C = 0.5$.

Cases for $\phi = 1.32$ and turbulent velocity, u', of 1 and 3 m/s are presented in Figure 5. Despite the general agreement obtained is rather good for both curves, for the first milliseconds the deviations from the experimental points are significant. This could, for instance, be attributed to the lack of specifications of the experimental ignition parameters.

5 CONCLUSIONS

An ignition model called ISSIM has been adapted to a RANS code and successfully implemented in OpenFOAM®. The model was tested in stagnant and turbulent cases to check its performance after the variation of different parameters, from which the following observations are drawn:

- The model is seen to overpredict the initial burned mass applied to the mixture. This was remedied by the incorporation of thicknesses factors set to match experimental values.
- An ad-hoc coefficient proposed to increase the burning velocity during spark timing greatly improved the general agreement with the experiments. Particularly, the model

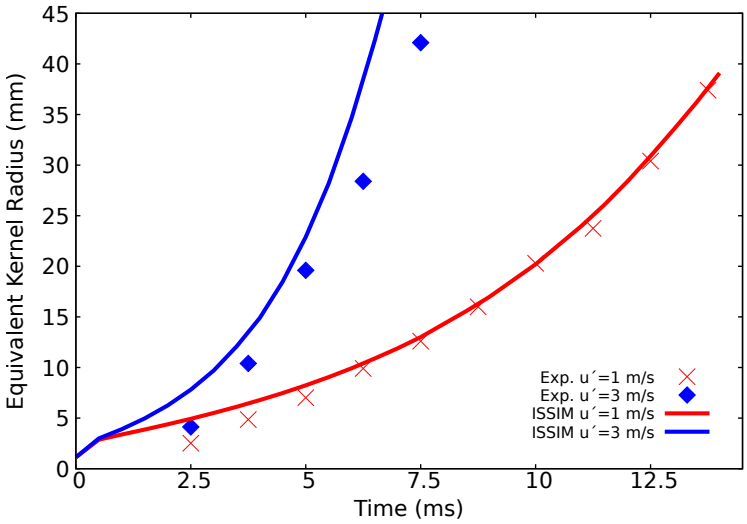

Figure 5: Effect of turbulence on temporal growth of flame kernel radii.

is currently able to correctly predict changes in ignition energy and power, equivalence ratio and turbulence intensity.

- With the incorporation of the ad-hoc coefficients described in Section 4, more tests should be conducted with the model in order to be used with confidence. These should include several distinct fuels and data from other researchers and bombs, to asseverate its generality.

ACKNOWLEDGMENTS

This work has received financial support from Consejo Nacional de Investigaciones Científicas y Técnicas (CONICET, Argentina), Universidad Nacional del Comahue (UNCo, Argentina, grant PIN 04/I-215), and Agencia Nacional de Promoción Científica y Tecnológica (ANPCyT, Argentina, grants PICT 2015-2904, PICT 2016-0105), and was partially performed with the Free Software Foundation GNU-Project resources as GNU/Linux OS, GCC compilers, GNU/Octave, and GNUPlot, as well as other Open Source resources as OpenFOAM®, ParaView, and LaTeX, among many others.

REFERENCES

Adelman H.G. A time dependent theory of spark ignition. *Symposium (International) on Combustion*, 18(1):1333–1342, 1981.

Amirante R., Distaso E., Tamburrano P., and Reitz R.D. Laminar flame speed correlations for methane, ethane, propane and their mixtures, and natural gas and gasoline for spark-ignition engine simulations. *International Journal of Engine Research*, 18(9):951–970, 2017.

Boudier P., Henriot S., Poinsot T., and Baritaud T. A model for turbulent flame ignition and propagation in piston engines. *Symposium (International) on Combustion*, 24(1):503–510, 1992.

Bradley D., Gaskell P.H., and Gu X.J. Burning velocities, Markstein lengths, and flame quenching for spherical methane-air flames: A computational study. *Combustion and Flame*, 104:176–198, 1996.

Bradley D., Gaskell P.H., and Gu X.J. The modeling of aerodynamic strain rate and flame cur-

vature effects in premixed turbulent combustion. *Symposium (International) on Combustion*, 27(1):849–856, 1998.

Bradley D., Haq M.Z., Hicks R.A., Kitagawa T., Lawes M., Sheppard C.G.W., and Woolley R. Turbulent burning velocity, burned gas distribution, and associated flame surface definition. *Combustion and Flame*, 133:415–430, 2003.

Choi C.R. and Huh K.Y. Development of a coherent flamelet model for a spark-ignited turbulent premixed flame in a closed vessel. *Combustion and Flame*, 114:336–348, 1998.

Colin O., Benkenida A., and Angelberger C. 3D modeling of mixing, ignition and combustion phenomena in highly stratified gasoline engines. *Oil & Gas Science and Technology - Rev. IFP*, 58(1):47–62, 2003.

Colin O. and Truffin K. A spark ignition model for large eddy simulation based on an FSD transport equation (ISSIM-LES). *Proceedings of the Combustion Institute*, 33:3097–3104, 2011.

Duclos J. and Colin O. Arc and Kernel Tracking Ignition Model for 3D Spark-Ignition Engine Calculations. In *COMODIA*, pages 343–350. Tokyo, 2001.

Duclos J.M., Veynante D., and Poinsot T. A comparison of flamelet models for premixed turbulent combustion. *Combustion and Flame*, 95:101–117, 1993.

Ge H. and Zhao P. A comprehensive ignition system model for spark ignition engines. *Proceedings of the ASME 2018*, ICEF2018-9574, 2018.

Issa R. Solution of the implicitly discretised fluid flow equations by operator-splitting. *Journal of Computational Physics*, 62(1):40–65, 1986.

Ko Y., Anderson R., and Arpaci V.S. Spark ignition of propane-air mixtures near the minimum ignition energy: Part I. An experimental study. *Combustion and Flame*, 83:75–87, 1991.

Launder B.E. and Spalding D.B. The numerical computation of turbulent flows. *Computer Methods in Applied Mechanics and Engineering*, 3(2):269–289, 1974.

Lewis B. and Vol Elbe G. *Combustion, Flames and Explosions of Gases*. Academic Press, 3 edition, 1987.

Lim M.T., Anderson R.W., and Arpaci V.S. Prediction of spark kernel development in constant volume combustion. *Combustion and Flame*, 69:303–316, 1987.

López E., Aguerre H., Pairetti C., Márquez Damián S., Gimenez J., and Nigro N. Contrastación de modelos para combustión premezclada en aplicaciones de motores de combustión interna. In *Jornadas Iberoamericanas de Motores Térmicos y Lubricación*, pages 295–308. La Plata, Argentina, 2016.

Lucchini T., Cornolti L., Montenegro G., D'Errico G., Fiocco M., Teraji A., and Shiraishi T. A comprehensive model to predict the initial stage of combustion in SI engines. *SAE Technical Paper*, 2013-01-1087, 2013.

Meneveau C. and Poinsot T. Stretching and quenching of flamelets in premixed turbulent combustion. *Combustion and Flame*, 86:311–332, 1991.

Mouriaux S. *Large Eddy Simulation of the turbulent spark ignition and of the flame propagation in spark ignition engines*. Ph.D. thesis, Université Paris-Saclay, 2016.

Pashley N., Stone R., and Roberts G. Ignition system measurement techniques and correlations for breakdown and arc voltages and currents. *SAE Technical Paper*, 2000-01-0245, 2000.

Patankar S.V. *Numerical Heat Transfer and Fluid Flow*. Taylor & Francis, 1980.

Poinsot T. and Veynante D. *Theoretical and Numerical Combustion*. Poinsot T. and Veynante D., 3 edition, 2012.